# Visualization of 3D Hyperspectral Soil Mapping Data via Autoencoder-based Clustering

Jianxin Sun, Xinyan Xie, Yu Pan, Yakub Islamov, Yufeng Ge, Hongfeng Yu
*University of Nebraska-Lincoln, Lincoln, NE, USA*

***Abstract*—Soil measurement and evaluation are crucial to various aspects of agriculture, including agricultural productivity, nutrient management, water management, and pH Regulation. Hyperspectral imaging is an advanced technique used to capture and analyze a wide range of light wavelengths (or spectral bands) across the electromagnetic spectrum. Hyperspectral imaging in soil research involves the use of this advanced imaging technique to analyze the spectral properties of soils. It allows researchers to capture detailed information about the composition, texture, and conditions of soil across a wide range of wavelengths in the electromagnetic spectrum. This in-depth spectral analysis provides valuable insights for studying soil health, nutrient content, moisture levels, and other critical parameters. However, existing hyperspectral analysis of soil relies on using imaging systems to exclusively capture information from the soil surface. This yields a two-dimensional image in which each pixel represents a spectrum vector. In this paper, we provide a new 3D hyperspectral data capturing features deep into the soil where each voxel represents a spectrum vector. For effective analysis of this type of new hyperspectral data, we develop a 3D visualization tool to not only directly visualize individual spectrum of the soil volume but also provide a way to cluster such high dimensional data leveraging a deep learning-based method through autoencoder.**

***Index Terms*—hyperspectral, 3D visualization, soil, deep learning, clustering**

## I. Introduction

Hyperspectral imaging is an effective tool in agricultural research for its ability to capture a wide range of wavelengths across the electromagnetic spectrum [18]. This technology provides detailed spectral information about crops and soil, which is crucial for various applications in agriculture, like crop health assessment, nutrient management, soil health assessment, and precision agriculture [17], [27], [41]. Hyperspectral imaging captures a wide range of wavelengths, providing detailed spectral information about objects or scenes. This enables the differentiation of materials based on their unique spectral signatures [15]. It also allows for the precise identification and discrimination of materials, substances, or features that may be challenging to distinguish using traditional imaging methods. However, it is challenging to directly visualize hyperspectral data. Hyperspectral data typically consists of hundreds to thousands of spectral bands. Visualizing such high-dimensional data in a meaningful and interpretable way is nontrivial. Hyperspectral datasets can be quite large in size, especially when collected over a wide spatial or temporal domain. Visualizing such a large volume of data can be computationally demanding. It's easy to overwhelm viewers with an excessive amount of information. It is crucial to effectively represent such high-dimensional information through dimension reduction methods [22].

Volume visualization is a method employed in computer graphics and scientific visualization to depict and present three-dimensional (3D) data in a manner that is easily comprehensible and meaningful [14]. It proves especially valuable in illustrating intricate structures and phenomena characterized by depth and spatial scope, including but not limited to medical imaging data, scientific simulations, as well as geological and environmental datasets [44]. Intrinsic structure and features can be displayed using various visualization techniques to provide insights to help scientists better understand the dataset. Volume rendering and isosurface rendering are popular tools for visualizing datasets in a 3D spatial domain. Although volume visualization can visualize 3D datasets like 3D hyperspectral soil mapping data, it can only generate the rendering from a scalar field. A typical hyperspectral vector normally has thousands of spectral bands, making traditional volume visualization raise bias in the analysis of 3D hyperspectral data.

In this work, we aim to tackle the challenge of visualizing 3D hyperspectral datasets. First, we design an effective web-based tool with a user interface for interactive volume visualization. Second, we provide a dimension reduction method using a deep learning-based autoencoder to map each hyperspectral sample to a lower-dimensional space. Third, the features learned in latent space are clustered into multiple groups based on similarity measurement so that the visualization of the clustered samples provides a comprehensive insight into the distribution of soil characteristics in 3D space. The main contributions of this work include:

- An effective tool for visualizing 3D hyperspectral datasets used for 3D soil mapping.
- Deep learning-based autoencoder network to learn the feature in a lower dimension.
- Sample clustering to review the distribution of similarity of the soil dynamics.

The subsequent sections of this paper are organized as follows: we first provide an overview of related work in Section II and the data collection of 3D hyperspectral soil mapping in Section III. Section IV outlines the methods used for feature space learning and clustering. Experimental results are presented in Section V. We draw our conclusions in Section VI.

## II. Related Work

### A. Hyperspectral Imaging

Hyperspectral imaging identifies spectral signals through a sequence of contiguous channels with a narrow spectral bandwidth. As a result, it can capture intricate spectral details of targets that might otherwise be overlooked or distorted [32]. Hyperspectral imaging has found extensive application in agricultural research for extracting diverse attributes related to crops and soil, including factors like chlorophyll content, biomass, yield, and soil quality [12], [24], [25], [34]. Hyperspectral imagery enables more precise and timely identification of the physiological condition of crops [9], [21]. In recent years, a diverse array of compact and affordable hyperspectral sensors have been created and are now accessible for commercial applications. This has led to their widespread utilization in a variety of monitoring tasks, whether mounted on manned or unmanned airborne platforms such as unmanned aerial vehicles (UAVs) [9], [19], [43]. By utilizing hyperspectral data, scientists have explored various agricultural attributes. These encompass sought-after factors like crop water content, leaf area index (LAI), chlorophyll and nitrogen levels, identification of pests and diseases, measurement of plant height, assessment of phenological information, determination of soil moisture, and evaluation of soil organic matter content [1], [39]. Existing soil research utilizing hyperspectral sensing are more rely on the measurements in 2D image space [13], [20], [30] where each pixel is a vector of intensities of all spectrum samples. However, there are sporadic research works targeting the measurement and analysis of 3D hyperspectral datasets where each voxel is a spectral intensity vector.

### B. Scientific Data Visualization

Scientific datasets are characterized by their 3D spatial domain and multidimensional nature. Volume visualization of scientific data is a technique used in computer graphics and imaging to represent and display three-dimensional (3D) data in a visually understandable and meaningful way [5], [44]. It is particularly useful for visualizing complex structures and phenomena that have depth and spatial extent, such as medical imaging data (e.g., CT scans, MRI), scientific simulations, and geological or environmental datasets [2], [14], [29], [33], [36], [37], [40]. Various algorithms have been devised by researchers to address volume visualization challenges in scientific data, including tasks like calculating isosurfaces, streamlines, and volume rendering with a focus on efficient I/O handling [4], [23]. By factoring in the distance between the camera view and individual data segments in the current view, multi-resolution techniques [35], [38] selectively load data segments at varying levels of detail. This strategy decreases the amount of data loaded for rendering while maintaining a similar level of rendering quality. Enhancing real-time access to raw data in visualization tasks like progressive slicing and particle traces can be achieved through methods such as employing an optimized disk data arrangement [28] or utilizing pre-computed lookup tables [6]. Although multidimensional data can be visualized at a high level leveraging multidimensional transfer functions [7], [16], [31], it is still a challenging task to effectively analyze 3D spacial volume with high-dimensional representations like hyperspectral vectors.

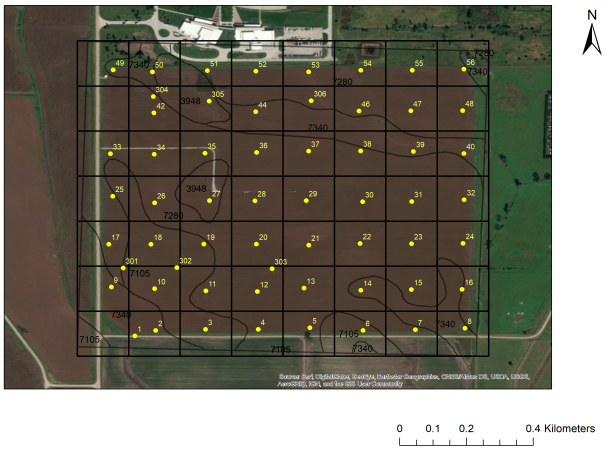


Fig. 1: Distribution of the measurement locations across the field of interest.

## III. 3D Hyperspectral Data

### A. Data Collection

The 3D hyperspectral data we obtained is a 3D soil volume measured at different spatial locations with various depths. The equipment we used is the visible and near-infrared (VisNIR) integrated multi-sensing penetrometer [26], [42] for in situ, high-resolution vertical soil sensing. The in situ soil VisNIR reflectance spectra, penetration resistance, and insertion depth are measured for each sample. Figure 1 shows the sampling location map with labels for the field of interest. The dimension of the sampling is 7 by 8 with a depth of 5, so the volume size of the dataset is $7 \times 8 \times 5$. For each sample, we measure 2151 hyperspectral samples across the spectrum. We also measured extra sample locations, like points labeled 301 and 302 in Figure 1, for verification purposes.

### B. Data Processing

Since the measurement for each sample point from the penetrometer is a comprehensive data collection on various metrics, the spectral data need to be extracted for our analysis. Our measurement failed to collect data on sample 41 due to the difficulty of practicing measurement of its specific location, we need to reconstruct the spectral information from its neighboring samples, 33, 42, and 49, through bilinear interpolation. We perform a similar interpolation on sample 1 for its existing measured location is off to the correct location. For volume visualization of the intensity of individual spectra, we create 2151 binary volumetric files for all samples on each spectrum with a spatial resolution of $7 \times 8 \times 5$. For training the autoencoder, as detailed in subsection IV-A, we also flatten the volumetric data into a collection of hyperspectral vectors

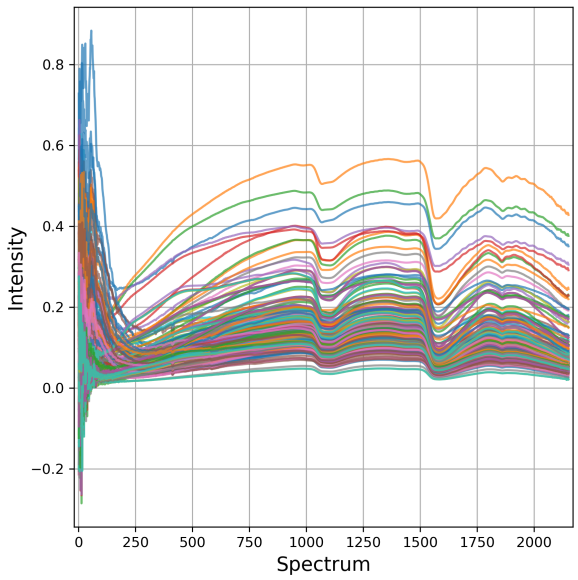


Fig. 2: All 280 hyperspectral vectors measured.

of size 280 ($7 \times 8 \times 5$). Figure 2 plots the intensities of all hyperspectral vectors.

## IV. Method

### A. Feature Space Learning

The architecture of the autoencoder is leveraged as the primary unsupervised learning technique for extracting features in the feature space, which has been widely used across various domains [10] for dimension reduction. A standard autoencoder is comprised of an encoder and a decoder. A low-dimensional feature space is extracted through the encoder part of the trained autoencoder network [3]. Multilayer perceptron (MLP) [8] is used as the fitting element to capture the dynamics of the encoder and decoder parts of the autoencoder network. A loss function is used to minimize the difference between the input of the encoder and the output of the decoder.

Figure 3 shows the detailed structure of the autoencoder used in our work for feature space learning. The input is the spectral vector of size 2151 measured for a particular sample in the soil. The autoencoder consists of 3 fully connected layers for both the encoding and decoding phases. 512, 128, and 32 neurons are used for the three layers of the encoder followed by the latent layer with 2 neurons. 32, 128, and 512 neurons are used for the three layers of the decoder to connect the latent layer to the output layer with the same size of 2151 as input. In our work, we set the latent space as a 2D space. We use ReLU as the activation function, and the mean squared errors (MSE) as a metric of the loss function between the input and reconstructed output.

### B. Clustering

Once the autoencoder network is trained, the parameters of the encoder are fixed and used for inferencing the latent space from the spectral vector of each sample. The distance

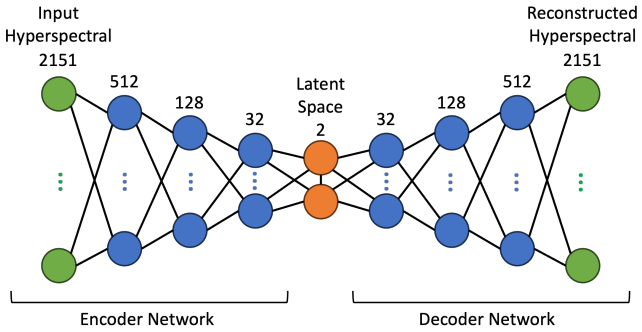


Fig. 3: The network structure of autoencoder.

measurement is the difference $Diff_{mn}$ between two samples $m$ and $n$ in latent space:

$$Diff_{mn} = |\mathbf{p}_m - \mathbf{p}_n|, \tag{1}$$

where $|\mathbf{p}_m - \mathbf{p}_n|$ is the Euclidean distance between the 2D latent space vectors $\mathbf{p}_m$ and $\mathbf{p}_n$. Based on the distance $Diff_{mn}$ between any two sample $m$ and $n$, the k-means algorithm is utilized to cluster all samples of the soil volume.

### C. Visualization

For volume visualization, we design a web-based interactive visualization user interface for volume rendering and isosurface rendering.

*1) Interactive Visualization:* Our rendering pipeline utilizes WebGL (Web Graphics Library), a powerful hardware-accelerated 3D graphics for web browsers, to harness the power of the GPU for responsive and interactive visualization.

*2) Cross-Platform Compatibility:* WebGL is supported by most modern web browsers, making it a cross-platform solution. This means that our visualization tool can run on a wide range of devices, including desktops, laptops, tablets, and even mobile phones.

*3) Lightweight:* Our visualization website is lightweight HTML with JavaScript for rendering using Graphics Library Shader Language (GLSL), making our tool not only effective but also efficient for visualizing volume data.

*4) User-friendly User Interface:* Figure 4 shows the user interface of our web-based volume visualization tool. a is the area showing the rendering image of the volume visualization. Users can select different color transfer functions by selecting colormaps from the drop-down menu in b. c shows a brief introduction about how to manipulate the view through mouse or touch movement for rotating, zooming, and panning. d is the loading status bar for showing how much data has been loaded to the website after the user selects a local volume file through e. f and g determined the value of the lower and upper bound of the opacity transfer function for intensity, which will selectively show the region of interest as desired. Once the user toggles the box in h, the relative position of lower (f) and upper bound (g) are fixed, this is used for visualizing the isosurface of various intensity values. This visualization tool is also capable of visualizing clustering results.

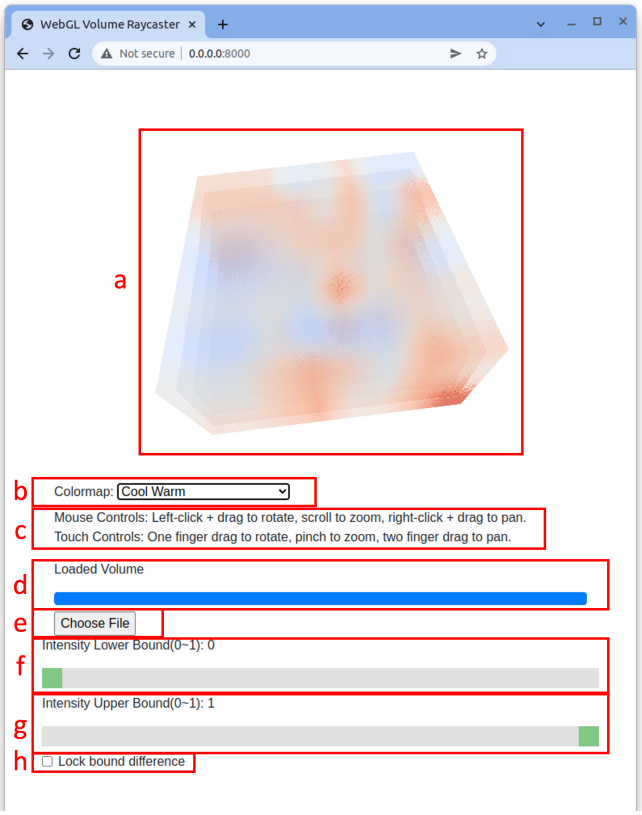


Fig. 4: Visualization UI for volume visualization of the intensity of a given spectrum of the soil volume. The UI can also visualize the clustering results.

To better understand the relation between samples within the same class, we leverage hierarchical edge bundling [11] to visualize the clustered results from a graph perspective.

## V. Results and Evaluation

We conduct experiments on key procedures of our pipeline for visualizing 3D hyperspectral soil mapping data.

### A. Experiment Setup

Our visualization tool is tested on a desktop platform with an Intel i7-7700K CPU, 16GB DDR4 DRAM 3200MHz, and Nvidia GTX 1050Ti GPU. We also perform testing on an Android phone with Qualcomm Snapdragon 660 (4 cores 2.2 Ghz and 4 cores 1.8 Ghz) and 4GB RAM. We use Google Chrome as the browser for both platforms for its support of WebGL 2.0.

### B. Training

The autoencoder network is trained using the PyTorch software stack to accelerate the training and inferencing performance on a single Nvidia GTX 1050Ti GPU. Adam optimizer is used to adjust the learning rate of the gradient descent. 10000 epochs are used to train the network. Figure 5 shows how the loss decreases for the first 100 epochs.

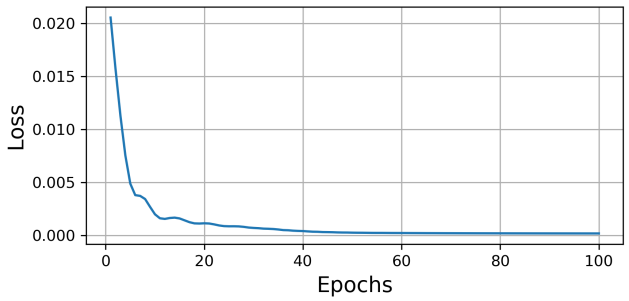


Fig. 5: How the loss changes as the training epoch increases.

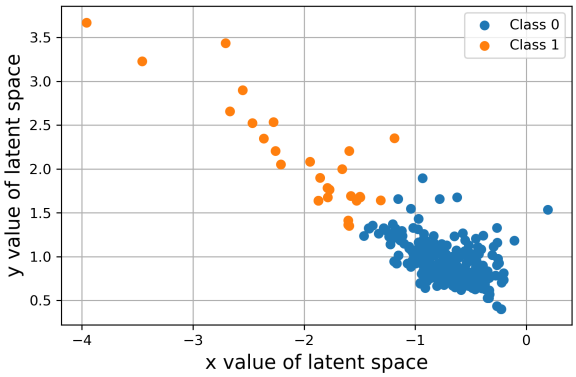


Fig. 6: 2 classes clustering in the latent space.

### C. Clustering

Once the autoencoder network is trained, the parameters of its encoder part are fixed for inferencing the latent representation for all spectral vectors. In this 2D latent space, we apply the k-means clustering algorithm to cluster the feature into various classes. Figure 6, Figure 7 and Figure 8 show the clustering of all the samples in the soil volume into 2, 3, and 4 groups. Based on the result of each clustering, we also generate a respective new volume with values reflecting the class index so that we can use our visualization tool to visualize the clustering results.

### D. Visualization

*1) Volume Visualization:* We first test the volume visualization of a specific spectrum of the value. Two popular types of visualization, volume rendering, and isosurface rendering, are tested for visualizing the 3D hyperspectral soil mapping data. Figure 9 lists the visualization results where the first column shows the volume rendering of the intensity for the 1th, 100th, and 1000th spectrum values. The second column shows the isosurface rendering of the intensity of 0.144 for the 1st, 100th, and 1000th spectrum values. Our tool provides an intuitive visualization that helps users better understand the structure and distribution of a specific spectrum value.

*2) Cluster Visualization:* The clustered results are also visualized using our tool for clustering 2, 3, and 4 groups as shown in Figure 10. The 4 classes are color-mapped into

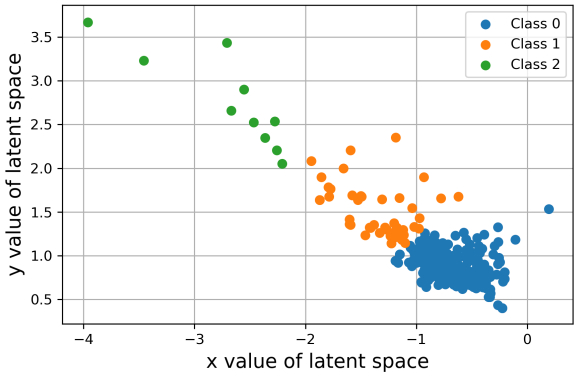


Fig. 7: 3 classes clustering in the latent space.

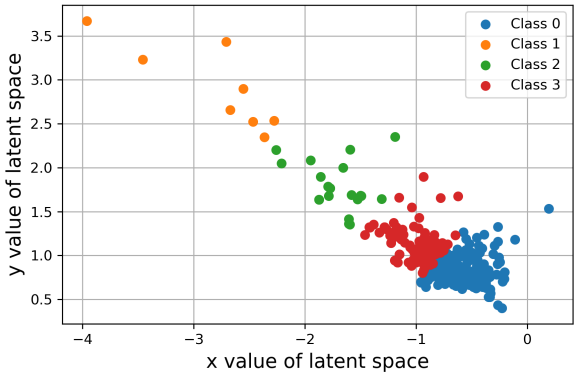


Fig. 8: 4 classes clustering in the latent space.

red, blue, green, and purple. We can see that our tool can clearly visualize the region of different clusters.

*3) Graph Visualization:* We also visualize clustering results as a graph where samples in the same class are connected with edges. Figure 11 shows the hierarchical edge bundling results on the clustering result for 4 classes. The numbers on the circle indicate the indices of the samples. Each subfigure in Figure 11 shows the bundled edges connecting the samples belonging to the same class so that we can clearly see the magnitude and the distribution of each class in the sample space.

## VI. Conclusions

We present a visualization pipeline to cluster and visualize 3D hyperspectral soil mapping data. A deep learning-based autoencoder neural network is used to learn a low-dimensional latent feature space. Clustering is performed on such latent space to segment the samples in soil volume based on their similarities. The proposed visualization tool is fast, cross-platform compatible, lightweight, and user-friendly. We perform experiments to show the results of volume visualization and cluster visualization, and test the effectiveness of the pipeline. We regard this work as an initial attempt to visualize 3D hyperspectral data effectively and efficiently. The performance of our tool scales with the input 3D volume size and its input latency is determined by the capability of the GPU hardware

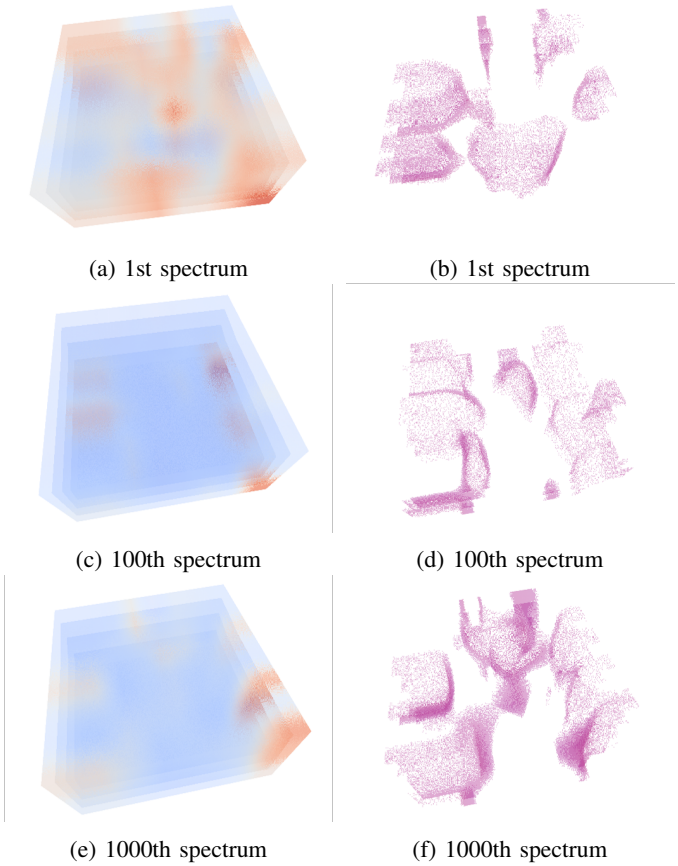

(a) 1st spectrum (b) 1st spectrum

(c) 100th spectrum (d) 100th spectrum

(e) 1000th spectrum (f) 1000th spectrum

Fig. 9: Volume visualization of the 3D hyperspectral soil mapping data. The first column shows the volume rendering results, while the second column shows the isosurface results.

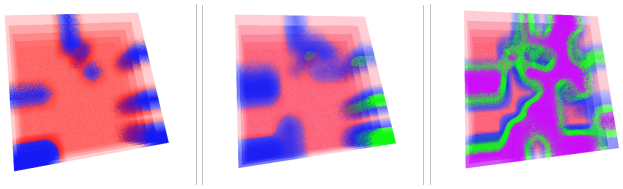

(a) 2 clusters (b) 3 clusters (c) 4 clusters

Fig. 10: Clustering visualization for clustering 2, 3, and 4 groups.

used on the user end. In the future, we would like to integrate various data models to represent data for handling large-scale hyperspectral volumes and overcoming the interpolation artifact of sparse 3D datasets. We are also interested in using other dimension reduction methods and comparing their performance on clustering.

## Acknowledgment

The work has been supported in part by the United States Department of Agriculture – National Institute of Food and Agriculture grant Award 2018-67007-28529 to Y.G. and H.Y., the National Science Foundation grant IIS-1652846, and the

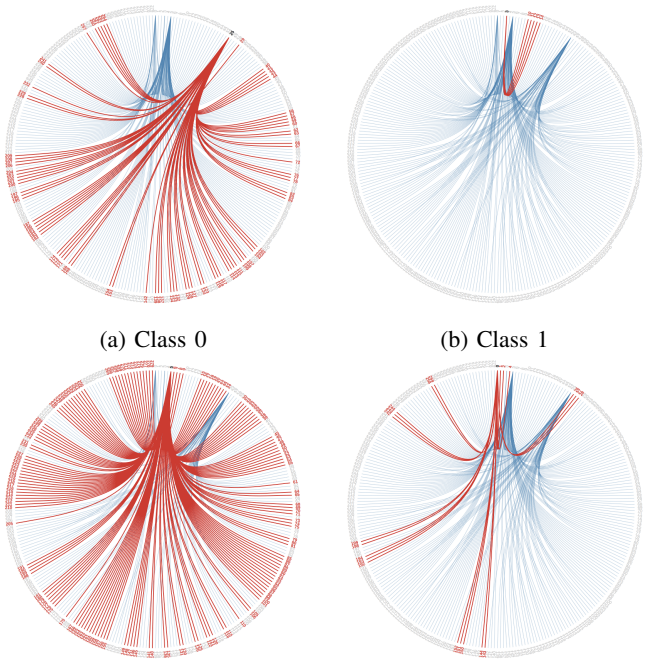

(a) Class 0 (b) Class 1

(c) Class 2 (d) Class 3

Fig. 11: Hierarchical edge bundling results on the clustering result for 4 classes.

Daugherty Water for Food Global Institute at the University of Nebraska.

## References


[1] T. Adão, J. Hruška, L. Pádua, J. Bessa, E. Peres, R. Morais, and J. J. Sousa. Hyperspectral imaging: A review on uav-based sensors, data processing and applications for agriculture and forestry. *Remote Sensing*, 9(11), 2017.

[2] I. Bahkali and S. K. Semwal. Medical visualization using 3d imaging and volume data: A survey. In *Proceedings of the Future Technologies Conference (FTC) 2020, Volume 3*, pages 251–261. Springer, 2021.

[3] Y. Bengio et al. Learning deep architectures for ai. *Foundations and trends® in Machine Learning*, 2(1):1–127, 2009.

[4] J. Beyer, M. Hadwiger, and H. Pfister. State-of-the-art in gpu-based large-scale volume visualization. *Computer Graphics Forum*, 34(8):13–37, 2015.

[5] K. Brodlie and J. Wood. Recent advances in volume visualization. *Computer Graphics Forum*, 20(2):125–148, 2001.

[6] R. Bruckschen, F. Kuester, B. Hamann, and K. I. Joy. Real-time out-of-core visualization of particle traces. In *Proceedings of the IEEE 2001 Symposium on Parallel and Large-Data Visualization and Graphics*, PVG '01, page 45–50. IEEE Press, 2001.

[7] S. dos Santos and K. Brodlie. Gaining understanding of multivariate and multidimensional data through visualization. *Computers & Graphics*, 28(3):311–325, 2004.

[8] M. W. Gardner and S. Dorling. Artificial neural networks (the multilayer perceptron)—a review of applications in the atmospheric sciences. *Atmospheric environment*, 32(14-15):2627–2636, 1998.

[9] V. Gonzalez-Dugo, P. Hernandez, I. Solis, and P. J. Zarco-Tejada. Using high-resolution hyperspectral and thermal airborne imagery to assess physiological condition in the context of wheat phenotyping. *Remote Sensing*, 7(10):13586–13605, 2015.

[10] R. Haggerty, J. Sun, H. Yu, and Y. Li. Application of machine learning in groundwater quality modeling - a comprehensive review. *Water Research*, 233:119745, 2023.

[11] D. Holten. Hierarchical edge bundles: Visualization of adjacency relations in hierarchical data. *IEEE Transactions on visualization and computer graphics*, 12(5):741–748, 2006.

[12] E. R. Hunt and C. S. T. Daughtry. What good are unmanned aircraft systems for agricultural remote sensing and precision agriculture? *International Journal of Remote Sensing*, 39(15-16):5345–5376, 2018.

[13] S. Jia, H. Li, Y. Wang, R. Tong, and Q. Li. Hyperspectral imaging analysis for the classification of soil types and the determination of soil total nitrogen. *Sensors*, 17(10):2252, 2017.

[14] J. Kehrer and H. Hauser. Visualization and visual analysis of multifaceted scientific data: A survey. *IEEE Transactions on Visualization and Computer Graphics*, 19(3):495–513, 2013.

[15] M. J. Khan, H. S. Khan, A. Yousaf, K. Khurshid, and A. Abbas. Modern trends in hyperspectral image analysis: A review. *IEEE Access*, 6:14118–14129, 2018.

[16] J. Kniss, G. Kindlmann, and C. Hansen. Multidimensional transfer functions for interactive volume rendering. *IEEE Transactions on Visualization and Computer Graphics*, 8(3):270–285, 2002.

[17] J. Li, N. K. Wijewardane, Y. Ge, and Y. Shi. Improved chlorophyll and water content estimations at leaf level with a hybrid radiative transfer and machine learning model. *Computers and Electronics in Agriculture*, 206:107669, 2023.

[18] B. Lu, P. D. Dao, J. Liu, Y. He, and J. Shang. Recent advances of hyperspectral imaging technology and applications in agriculture. *Remote Sensing*, 12(16), 2020.

[19] B. Lu, Y. He, and P. D. Dao. Comparing the performance of multispectral and hyperspectral images for estimating vegetation properties. *IEEE Journal of Selected Topics in Applied Earth Observations and Remote Sensing*, 12(6):1784–1797, 2019.

[20] Y. Lu, D. Perez, M. Dao, C. Kwan, and J. Li. Deep learning with synthetic hyperspectral images for improved soil detection in multispectral imagery. In *2018 9th IEEE Annual Ubiquitous Computing, Electronics & Mobile Communication Conference (UEMCON)*, pages 666–672, 2018.

[21] A. Lucieer, Z. Malenovský, T. Veness, and L. Wallace. Hyper-uas—imaging spectroscopy from a multirotor unmanned aircraft system. *Journal of Field Robotics*, 31(4):571–590, 2014.

[22] Y. Ma and L. Zhu. A review on dimension reduction. *International Statistical Review*, 81(1):134–150, 2013.

[23] F. Marton, M. Agus, and E. Gobbetti. A framework for gpu-accelerated exploration of massive time-varying rectilinear scalar volumes. *Computer Graphics Forum*, 38(3):53–66, 2019.

[24] N. G. Maxim Shoshany and A. Chudnovsky. Monitoring of agricultural soil degradation by remote-sensing methods: a review. *International Journal of Remote Sensing*, 34(17):6152–6181, 2013.

[25] H. McNairn, C. Champagne, J. Shang, D. Holmstrom, and G. Reichert. Integration of optical and synthetic aperture radar (sar) imagery for delivering operational annual crop inventories. *ISPRS Journal of Photogrammetry and Remote Sensing*, 64(5):434–449, 2009. Theme Issue: Mapping with SAR: Techniques and Applications.

[26] M. Murad, E. Jones, B. Minasny, A. McBratney, N. Wijewardane, and Y. Ge. Assessing a visnir penetrometer system for in-situ estimation of soil organic carbon under variable soil moisture conditions. *Biosystems Engineering*, 224:197–212, 2022.

[27] P. Pandey, Y. Ge, V. Stoerger, and J. C. Schnable. High throughput in vivo analysis of plant leaf chemical properties using hyperspectral imaging. *Frontiers in plant science*, 8:1348, 2017.

[28] V. Pascucci and R. J. Frank. Global static indexing for real-time exploration of very large regular grids. In *Proceedings of the 2001 ACM/IEEE Conference on Supercomputing*, 2001.

[29] N. Pradhan, V. S. Dhaka, G. Rani, V. Pradhan, E. Vocaturo, and E. Zumpano. Conditional generative adversarial network model for conversion of 2 dimensional radiographs into 3 dimensional views. *IEEE Access*, 2023.

[30] P. R. Robichaud, S. A. Lewis, D. Y. Laes, A. T. Hudak, R. F. Kokaly, and J. A. Zamudio. Postfire soil burn severity mapping with hyperspectral image unmixing. *Remote Sensing of Environment*, 108(4):467–480, 2007.

[31] C. T. Rueden and K. W. Eliceiri. Visualization approaches for multidimensional biological image data. *BioTechniques*, 43(1S):S31–S36, 2007. PMID: 17936940.

[32] R. N. Sahoo, S. S. Ray, and K. R. Manjunath. Hyperspectral remote sensing of agriculture. *Current Science*, 108(5):848–859, 2015.

[33] R. G. Sayre, D. J. Wright, S. P. Breyer, K. A. Butler, K. Van Graafeiland, M. J. Costello, P. T. Harris, K. L. Goodin, J. M. Guinotte, Z. Basher, et al. A three-dimensional mapping of the ocean based on environmental data. *Oceanography*, 30(1):90–103, 2017.

[34] J. Shang, J. Liu, B. Ma, T. Zhao, X. Jiao, X. Geng, T. Huffman, J. M. Kovacs, and D. Walters. Mapping spatial variability of crop growth

conditions using rapideye data in northern ontario, canada. *Remote Sensing of Environment*, 168:113–125, 2015.

[35] R. Sicat, J. Krüger, T. Möller, and M. Hadwiger. Sparse pdf volumes for consistent multi-resolution volume rendering. *IEEE Transactions on Visualization and Computer Graphics*, 20(12):2417–2426, 2014.

[36] J. Sun, D. Lenz, H. Yu, and T. Peterka. Mfa-dvr: direct volume rendering of mfa models. *Journal of Visualization*, pages 1–18, 2023.

[37] J. Sun, C. Wu, Y. Ge, Y. Li, and H. Yu. Spatial-temporal scientific data clustering via deep convolutional neural network. In *2019 IEEE International Conference on Big Data (Big Data)*, pages 3424–3429. IEEE, 2019.

[38] S. Suter, M. Makhynia, and R. Pajarola. Tamresh – tensor approximation multiresolution hierarchy for interactive volume visualization. *Computer Graphics Forum*, 32(3pt2):151–160, 2013.

[39] M. Teke, H. S. Deveci, O. Haliloğlu, S. Z. Gürbüz, and U. Sakarya. A short survey of hyperspectral remote sensing applications in agriculture. In *2013 6th International Conference on Recent Advances in Space Technologies (RAST)*, pages 171–176, 2013.

[40] J. N. Van Driel. Three dimensional display of geologic data. In *Three Dimensional Applications In GIS*, pages 1–9. CRC Press, 2020.

[41] N. K. Wijewardane, Y. Ge, S. Wills, and T. Loecke. Prediction of soil carbon in the conterminous united states: Visible and near infrared reflectance spectroscopy analysis of the rapid carbon assessment project. *Soil Science Society of America Journal*, 80(4):973–982, 2016.

[42] N. K. Wijewardane, S. Hetrick, J. Ackerson, C. L. Morgan, and Y. Ge. Visnir integrated multi-sensing penetrometer for in situ high-resolution vertical soil sensing. *Soil and Tillage Research*, 199:104604, 2020.

[43] P. J. Zarco-Tejada, L. Suárez, and V. González-Dugo. Spatial resolution effects on chlorophyll fluorescence retrieval in a heterogeneous canopy using hyperspectral imagery and radiative transfer simulation. *IEEE Geoscience and Remote Sensing Letters*, 10(4):937–941, 2013.

[44] Q. Zhang, R. Eagleson, and T. M. Peters. Volume visualization: a technical overview with a focus on medical applications. *Journal of digital imaging*, 24:640–664, 2011.